Deep-Sea Research I (2007) **54**(6) p.939–950.

Trace gas disequilibria during deep-water formation

Roberta C. Hamme*
School of Earth and Ocean Sciences, University of Victoria,
P.O. Box 3055 STN CSC, Victoria, BC V8W3P6, Canada

Jeffrey P. Severinghaus
Scripps Institution of Oceanography, University of California San Diego,
9500 Gilman Drive, Dept 0244, La Jolla, CA 92093-0244, USA

Abstract

We present high-precision measurements by a new isotope dilution technique of a suite of inert gases in the North Pacific. Remarkably smooth gradients in Ar, Kr and Xe from near equilibrium in intermediate waters to several percent undersaturated in deep waters were observed. The general pattern in the deepest waters was that Ar, Kr and Xe were undersaturated (Ar least and Xe most), while N_2 was close to equilibrium, and Ne was supersaturated. We propose that this pattern was produced by the interaction between the different physical properties of the gases (solubility and the temperature dependence of solubility) with the rapid cooling and high wind speeds that characterize deep-water formation regions. In a simple model of deep-water formation by convection, the saturations of the more temperature-sensitive gases were quickly driven down by rapid cooling and could not reequilibrate with the atmosphere before the end of the winter. In contrast, the gas exchange rate of the more bubble-sensitive gases (Ne and N_2) was able to meet or exceed the drawdown by cooling. Our simple convection model demonstrates that the heavier noble gases (Ar, Kr and Xe) are sensitive on seasonal timescales to the competing effects of cooling and air-sea gas exchange that are also important to setting the concentration of CO_2 in newly formed waters.

*Corresponding author. Tel.: +1-250-472-4014; Fax: +1-250-721-6200; E-mail: rhamme@uvic.ca

1 Introduction

In this paper, we present full-depth profiles of five inert, dissolved gases measured in the subtropical North Pacific. Argon, Kr and Xe have been measured by a new isotope dilution method and demonstrate previously unknown trends with depth. Our focus here is to explain the pattern in gas saturation observed in the deepest waters, where some gases are undersaturated and others supersaturated. (Saturation refers here to the percent difference between the actual concentration of a gas and the concentration at equilibrium with the atmosphere for the potential temperature and salinity of the water.)

One motivation for measuring inert gases is that they may provide a constraint over the efficiency of the carbon solubility pump (Archer, 2003), in which cooling waters create undersaturations that drive CO_2 uptake. These undersaturations occur because CO_2 and most other gases are more soluble at colder temperatures, within the range 0–40^{o}C. The non-anthropogenic CO_2 sink observed in the North Atlantic has been partially attributed to this solubility pump (Takahashi et al., 1995), and modeling studies have shown that rapidly cooling waters do not fully equilibrate with the atmosphere because of the slow kinetics of air-sea CO_2 exchange (Sarmiento et al., 1995; Toggweiler et al., 2003). Considerable differences exist among models in their treatment of the solubility pump (Archer et al., 2000), which adds uncertainty to their predictive capabilities, particularly in the response

of carbon uptake to changing ocean circulation and in the cause of glacial/interglacial CO_2 changes. Determining the strength of the solubility pump directly from observations of carbon is a challenge, due to the strong biological overprint of photosynthesis and respiration. We argue here that the undersaturation observed in the heavier inert gases is caused by rapidly cooling waters that do not fully equilibrate with the atmosphere, a key factor in the inefficiency of the carbon solubility pump.

It has been recognized for some time that the properties of inert gases give them the potential to act as powerful tracers of physical processes in the ocean (Benson and Parker, 1961; Bieri, 1971; Craig and Weiss, 1971). Recent analytical improvements are allowing geochemists to take better advantage of the information recorded by these tracers, the power of which arises from the range in physical properties among the gases. The properties of the noble gases we measured follow a clear progression from the light (Ne) to heavy (Xe) gases, with the heavier gases being generally more soluble and having a greater temperature dependency to their solubilities (Figure 1). Nitrogen is a special case; its solubility is more similar to that of Ne, while its degree of temperature dependence is very similar to that of Ar (Hamme and Emerson, 2004b).

Colder water can hold more of these dissolved gases at equilibrium with the atmosphere, so cooling will act to reduce the saturation of these gases. The more rapidly a water mass cools, and the more sensitive a specific gas is to temperature, the more unlikely that air-sea gas exchange will be able to counteract cooling and return the gas saturation to equilibrium. Therefore, we expect the saturations of the heaviest, most temperature-sensitive gases (Xe and Kr) to be most affected by rapid temperature change.

When breaking waves push bubbles of air beneath the surface, the partial pressure gradient from the gas in the bubble to the dissolved gas in the water is increased. This increased gradient usually causes a flux into the water, and may cause the gases to be supersaturated at steady-state (Fuchs et al., 1987; Jenkins, 1988; Woolf and Thorpe, 1991). Bubble-mediated gas exchange, particularly from smaller collapsing bubbles, will increase the saturation of the low solubility gases more, because the amount of these gases already dissolved in the water is quite small (Figure 1c). In our suite, the saturations of the least soluble gases (Ne and N_2) will be most affected by bubbles.

A change in atmospheric pressure affects the partial pressure gradient between the atmosphere and the ocean, and should affect all the dissolved gases equally. Many deep-water formation sites are characterized by persistent low barometric pressure, such as the Icelandic Low and the low around Antarctica. We reference gas saturations to 1 atm of pressure, so an atmospheric low will cause dissolved gases in equilibrium with that atmosphere to appear undersaturated.

In this paper, we compare our deep-water observations with a model of how convection in the Labrador Sea would be expected to affect dissolved gases. Only a very small component of deep Pacific water likely forms in the Labrador Sea, but extensive observations of this area (Lab Sea Group, 1998) have helped us to create a simple model that captures the first order effect of convection on gases. We use this model more as a thought experiment for investigating the dissolved gas pattern that may be produced by deep convection, not because we would expect a model of Labrador Sea convection to exactly reproduce the gas saturations measured in the deep Pacific. Previous measurements of Ne, N_2, and Ar in the deep Atlantic do show the same pattern we observe in the deep Pacific with Ne supersaturated, N_2 close to equilibrium and Ar undersaturated (Hamme and Emerson, 2002), so the observed pattern in the deep Pacific may hold throughout the deep ocean.

2 Analytical Methods

We measured depth profiles of Ar, Kr and Xe concentrations by a new method on samples collected at station ALOHA ($22^o45'$N 158^oW) in August 2004 (HOT 162, Fujieki et al. (2006)). Station ALOHA is located in the central region of the North Pacific Subtropical Gyre, about 100 km north of Oahu (Karl and Lukas, 1996). N_2 concentrations were derived from a N_2/Ar profile measured in June 2001 at the same location (HOT 127, Fujieki et al. (2004)) and the Ar concentrations measured in August 2004. Neon concentrations were also measured on the June 2001 cruise. While surface saturations for these two cruises are not directly comparable, we do not expect and have not observed seasonal variability in deep Ne or N_2/Ar saturations (Hamme, 2003).

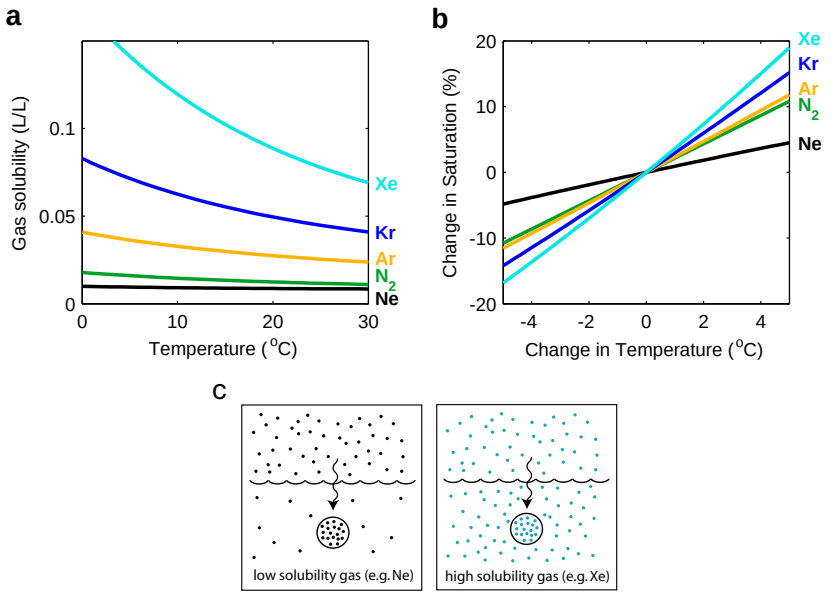

Figure 1: (a) Liters of pure gas at 1 atm that will dissolve in 1 L seawater at the given temperature (Bunsen solubilities). (b) The change in gas saturation that will result from a given warming or cooling of 5^{o}C seawater. This example does not take gas exchange processes into account. (c) Illustration of why bubble-mediated gas exchange affects the saturation of low solubility gases more.

The new method measures total Ar concentration by isotope dilution, and Kr and Xe concentrations by ratio with Ar. At sea, water was sucked from Niskin bottles into evacuated, 160-mL, glass flasks until they were half full. Back at the lab, the water was equilibrated with the flask headspace at a constant temperature, resulting in >90% of the formerly dissolved gases moving to the headspace. After equilibration, the water was drained leaving the gas phase undisturbed. (See Emerson et al. (1999) for a full description of the sampling and equilibration methods.) The gas sample was then transferred through a trap immersed in -100 ^{o}C ethanol to remove water and frozen into a long dip tube immersed in liquid helium. Helium in the sample is not quantitatively collected by this method. Next, the reactive gases (largely N_2 and O_2) were removed by exposure to a 900 ^{o}C Zr/Al gettering material (SAES Getters St101). The remaining noble gases were frozen into a new dip tube immersed in liquid helium. An aliquot of ^{38}Ar spike and an amount of N_2 (Airgas, 99.999% purity) equal to ten times the noble gas pressure were then frozen into the same dip tube to combine the gases. After warming of the sample tube to room temperature and several hours of sample homogenization, ^{36}Ar-^{38}Ar-^{40}Ar isotopes were simultaneously measured on a Finnigan MAT 252 stable isotope ratio mass spectrometer, followed by ^{84}Kr/^{36}Ar and ^{132}Xe/^{36}Ar ratios measured by peak jumping. (See Severinghaus et al. (2003) for a full description of the gas purification and mass spectrometry methods.) We estimate the precision of our method from the pooled standard deviation of the duplicate field samples collected at all depths. This precision was 0.15–0.17% for all three gases, with the precision of the gas ratios better at 0.04% for Kr/Ar and 0.07% for Xe/Ar.

The bulk of the ^{38}Ar spike used in this method (Oak Ridge National Laboratory, >95% isotopic enrichment) was held at a pressure of almost 1 Torr (125 Pa) in a 1800-mL stainless steel standard can with two bellows valves that formed a 1.2-mL aliquoting pipette (Severing-

Table 1: Magnitudes of the possible systematic offsets in the method

Possible source of error	Nominal size and error	Effect on saturation		
		Ar	Kr	Xe
Baratron pressure gauge	600 $\pm$ 0.9 Pa	0.15%	0.15%	0.15%
Ar solubility	$\pm$ 0.13%	0.13%	-	-
Kr solubility	$\pm$ 0.45%	-	0.45%	-
Xe solubility	$\pm$ 2%	-	-	2%
Ar spike abundances	$\pm$ 0.52%	-	0.19%	0.19%
Ar mole fraction in air	0.9343 $\pm$ 0.0006%	-	0.05%	0.05%
^{40}Ar/^{38}Ar ratio of standard	$\pm$ 0.5%	-	0.05%	0.05%
mass spec background	-0.49 $\pm$ 0.13mV	-	0.02%	0.5%

The following possible sources of error were judged to have a 0.02% or less effect on gas saturations: Kr & Xe mole fractions in air, sample preservation, flask volume, sample mass, thermometer calibration, Ar isotope fractionation, gas non-ideality during spike addition, and natural isotopic abundances.

haus et al., 2003). We achieved better reproducibility in the addition of spike aliquots to the samples by immersing the can and aliquoting pipette in a water bath to keep them at the same temperature. The amount of spike delivered in the aliquots was calibrated by reverse isotope dilution, a procedure in which a sample is used to calibrate the concentration of an isotopic spike. The pressure and temperature of dry air, collected either outside as described in Severinghaus et al. (2003) or from a specially prepared tank, was measured in a known volume immersed in a water bath to provide temperature stabilization. Moles of air used in the reverse isotope dilution procedure could then be calculated from the ideal gas law. These precise amounts of air were mixed with spike aliquots, processed, and analyzed as normal samples.

We evaluated the accuracy of the method by considering the possible sources of uncertainty that could have led to systematic offsets in our measurements (Table 1). We calibrated the 10 Torr pressure gauge (MKS Instruments 121AA-00010A Baratron) used to determine the pressure of the air for reverse isotope dilutions using the vapor pressure of water at the triple point (Lide, 2002). Based on multiple calibrations and the capabilities of these gauges, we think we were able to achieve an accuracy of $\pm$0.15% in the pressure measurement. Errors in the known solubilities of these gases have a direct effect on the saturation values. The use of reverse isotope dilution to calibrate the ^{38}Ar spike and the forward isotope dilution to measure the samples caused many of the possible sources of error to cancel for Ar but not for Kr and Xe. Uncertainty in the background value for the Faraday Cup detector used to measure Xe had an important effect. The Xe/Ar ratio in air is small and 3-4 times smaller than in seawater, which resulted in low raw voltages measured for air standards (17-18mV for ^{132}Xe). We estimated that this may have caused up to a $\pm$0.5% offset in our Xe measurements for HOT 162, but that we will be able to reduce this in the future with enhanced standardization protocols. We could not detect an effect due to non-linearities in the mass spectrometric measurement of the very different gas ratios in the air standards and in the water samples.

Water samples for Ne and N_2/Ar were collected in a similar way in 2001. Neon concentrations were measured by isotope dilution using a ^{22}Ne spike and a quadrupole mass spectrometer (Hamme and Emerson, 2004a). Nitrogen/argon ratios were measured on a Finnigan MAT 251 stable isotope ratio mass spectrometer at the University of Washington (Emerson et al., 1999). Errors were estimated at $\pm$0.17% precision and $\pm$0.18% accuracy for the Ne saturation and $\pm$0.08% precision and $\pm$0.01% accuracy for

the N_2/Ar ratio (Hamme and Emerson, 2006).

Gas saturations in this paper are calculated from the potential temperature and salinity of the sampled water and the solubility curves of Hamme and Emerson (2004b) for Ne, N_2 and Ar, and Weiss and Kyser (1978) for Kr. The solubility of Xe in seawater is not well known. Wood and Caputi (1966) measured Kr and Xe solubility at three temperatures in fresh and saltwater. Their freshwater Xe values were generally several percent higher than those measured by Benson and Krause (1976). Several percent differences also exist between the Wood and Caputi (1966) Kr solubility measurements and those of Weiss and Kyser (1978) and Benson and Krause (1976). Using a curve fit to the Wood and Caputi (1966) Xe data (Hamme and Emerson, 2004b), we found that Xe saturations calculated for our HOT 162 data were much lower than the results from the other gases would have suggested, based on the temperature sensitivity of the different gases. To bring the Xe saturations in-line with the other gases, we decreased the Wood and Caputi (1966) solubility curve by 2.0% to calculate Xe saturations. We plan to redetermine the Xe solubility curve in the near future to improve the accuracy of Xe saturation measurements. Supersaturations in this paper are referenced to an atmospheric pressure of 1 atm, including the vapor pressure of water saturated at the potential temperature of the water sample.

3 Data

In the deep Pacific, at station ALOHA, the gases show a distinctive pattern with the more soluble and temperature-dependent gases (Xe, Kr and Ar) being undersaturated and the less soluble gases (N_2 and Ne) being near equilibrium or supersaturated (Figure 2). At this location, the salinity minimum characterizing North Pacific Intermediate Water (NPIW) is found at 500m (Bingham and Lukas, 1996). Water below about 1600m is not ventilated within the North Pacific, but rather in the Southern Ocean or North Atlantic (Talley, 1997). This is the depth range at which the gas profiles are the most divergent from each other, suggesting that deep-water formation processes must be affecting each gas quite differently. Hamme and Emerson (2002) used a quasi-steady-state box model to show that temperature change and air-sea gas exchange, by both diffusive and bubble-mediated mechanisms, were likely the most important controls on gas distributions during water-mass formation. In this paper, we use a more sophisticated, time-dependent model of deep convection to explore the source of these patterns in more detail.

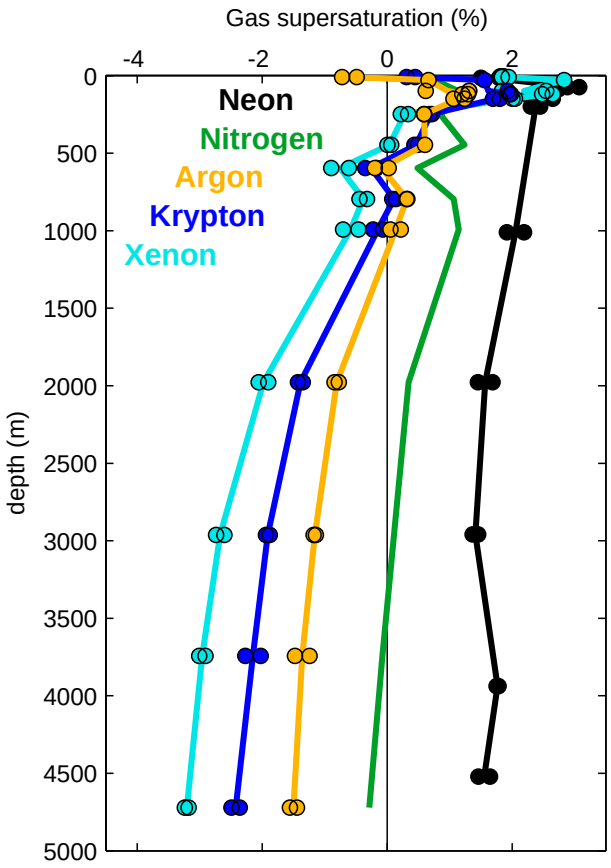

Figure 2: Depth profiles of Ne, N_2, Ar, Kr and Xe supersaturations (in %) measured at station ALOHA. Equilibrium with the atmosphere is indicated by the vertical line at 0%. Points indicate individual samples while the lines are the average of duplicates. Individual samples are not plotted for N_2 because these data are a combination of N_2/Ar ratio and Ar concentration measurements from different cruises and somewhat different depths. Xe supersaturations were increased by 2% above the solubility data of Wood and Caputi (1966).

Beyond the overall pattern in gas saturations observed in the deep water, the profiles also show interesting structure. In the core of the NPIW, Ar and Kr are close to equilibrium. From 800m to the bottom of the profile, Ar, Kr and Xe become steadily more undersaturated in a very smooth trend. This trend is unlikely to be the result of a sampling artifact that involves progressive alteration of gas concentrations in Niskin bottles on deck, because the deepest two samples (3800 and 4800m, with the 4800m bottle sampled first) were collected from a different cast than the 600-3000m samples (3000m bottle sampled first). This very smooth trend was not observable with our previous method of measuring Ar saturations, which combined O_2 concentration and O_2/Ar ratio measurements to determine Ar concentrations (Emerson et al., 1999). With that method, low O_2 concentrations below the euphotic zone contributed to larger errors in our titration measurements of O_2, which negatively affected the Ar precision as well.

Near the surface the gases are supersaturated or near saturation, with a clear subsurface peak in all the gases at about 100m. The points at 10 m and 600 m are more undersaturated than the data at nearby depths, possibly due to a sampling artifact. Both the 10- and 30-m points are within the mixed layer (40m depth), but the 30-m point is supersaturated in all the gases. Our duplicates at 10- and 600 m were within normal precision, and a similar Ar isotope dilution method and the original O_2/Ar ratio method also showed unusually low saturations for samples collected from these same Niskin bottles at 10 and 600m (S. Emerson personal communication). Summertime mixed layer Ar, measured by the previous O_2/Ar method, has never before been observed to be undersaturated at this location (Emerson et al., 1997; Hamme, 2003). Oxygen measurements in the 10m Niskin bottle were also anomalously low. Although we keep Niskin bottles closed until sampling to prevent contamination by a headspace, both depths were sampled last on their respective casts and the 600m sample had warmed by almost 10 ^{o}C. While these results may indicate some real process at work, we believe it is more likely that further improvements to our sampling methods remain to be made.

The primary controls on the deep trend and shallower features are not yet clear. The subsurface peak at $\sim$100m is strongest in the saturations of the most temperature-sensitive gases (Kr and Xe). This peak almost certainly results from solar heating of the waters beneath the mixed layer, an effect observed at this location in the summer for Ne, N_2 and Ar (Hamme, 2003), documented for Ar near Bermuda (Spitzer and Jenkins, 1989), and for Ne in the South Atlantic and Pacific (Well and Roether, 2003). Processes that likely play a role in setting gas saturations in the deeper thermocline include surface processes like rapid temperature change and gas exchange prior to subduction, mixing along and across isopycnals (Ito and Deutsch, 2006), and subsurface solar heating of water after subduction. The relative importance of these remains to be seen.

4 Model Results and Discussion

We constructed a simple, one-dimensional, time-dependent model of one winter's convection in the Labrador Sea, based on data from the 1996-97 Labrador Sea Convection Experiment (Lab Sea Group, 1998), to simulate the effect of deep-water formation processes on dissolved gases. The model had a well-mixed layer at the top, which was forced to deepen as it became denser than the layer beneath it through loss of heat to the atmosphere. The mixed layer remained relatively shallow until mid-January, when salinity stratification was overcome and the water column began to deepen rapidly (Figure 3). Diffusive and bubble-mediated gas exchange were modeled as independent processes driven by NCEP-modified wind speeds. Gas saturations were initially set to equilibrium with 1 atm pressure and allowed to iteratively evolve over several winters. (See Appendix A for a full description of the model and initial conditions.)

This model of the evolution in mixed-layer gas saturations over a winter of convection was successful at reproducing the observed pattern of dissolved gases in the deep ocean (Figure 4a). Bubble fluxes were tuned to reproduce the Ne supersaturation, but no other process in the model was tuned to create a match with the gas observations. Model mixed-layer supersaturations departed from their initial equilibrium condition within a few weeks and were quite variable during the first half of the winter when the mixed layer was shallow. When convection began in late January, mixed-layer supersaturations stabilized as large quantities of subsurface water were entrained into the mixed layer.

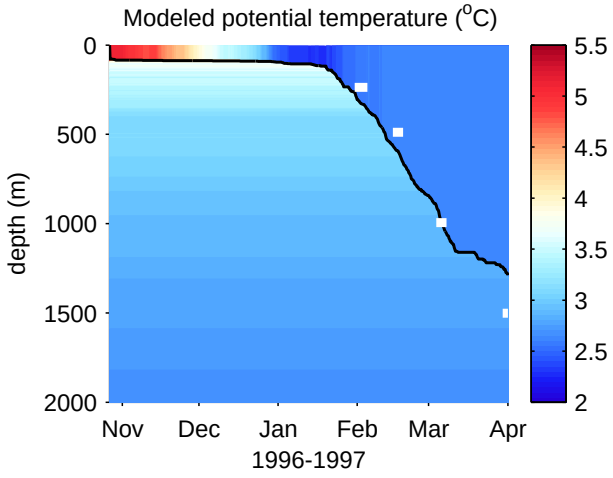

Figure 3: Contour plot of the potential temperature (^{o}C) of the model's water column over the 1996-97 winter. The black line shows the mixed layer depth. White rectangles show the approximate time that the mixed layer reached sensor depths at the Bravo mooring (Lab Sea Group, 1998).

By removing different processes from the model, we can evaluate their importance in creating the observed patterns in gas saturation. This approach does not evaluate possible interactions between processes, but given the small departures from equilibrium, we believe these are secondary effects. Holding the model atmospheric pressure at 1 atm rather than at the sea level pressure from the modified-NCEP data caused the final gas saturations to all be about 1% higher but had no effect on the degree of separation between the gases (Figure 4b). Preventing both diffusive and bubble-mediated gas exchange illustrates the effect that temperature change alone has on the gases. This effect was most dramatic in the first half of the winter when the mixed layer was shallow and cooling rapidly. Final gas saturations were all undersaturated and displayed a pattern similar to their temperature dependencies (Figure 4c). Preventing the gas saturations from responding to temperature change had a profound effect on the temperature sensitive gases. Note the almost complete absence of separation between Ar, Kr and Xe in Figure 4d, quite unlike the observations. Finally, the rate of bubble-mediated gas exchange had a profound effect on the insoluble gases (Ne and N_2, Figures 4e-f). When gas exchange through bubbles was prevented, only a tiny separation between Ar and N_2 was observed, again unlike the observations. A small amount of separation between Ne and Ar was still present without bubbles, because of these gases' different temperature dependencies. Doubling the bubble-mediated gas exchange rate resulted in very large increases in Ne and N_2.

This model demonstrates the predominant influence of rapid cooling and bubbles in producing the pattern of gas saturations we observe in the deep ocean. Diffusive gas exchange is important in modulating the influence of these other processes by forcing gas saturations back toward atmospheric equilibrium. Both low atmospheric pressure and rapid cooling are capable of causing gases to become undersaturated, but only rapid cooling can cause the percent level separation between Ar and Kr supersaturations that we observe. Local atmospheric pressure can be expected to alter the saturations of all the gases equally, but not to affect their ratios. The large separations observed between N_2 and Ar and between Ne and Ar supersaturations in deep waters demonstrates the importance of bubble-mediated gas exchange in setting the gas concentrations in the deep sea. Injection of bubbles is the only known process involved in open ocean convection that can create the separation between N_2 and Ar. Denitrification can also increase N_2 levels relative to Ar, but this process is limited to low O_2 regions (Codispoti et al., 2001).

While rates of cooling, wind speeds, and stratification will vary between areas of water mass formation, we expect convection anywhere to produce similar patterns in these gases with Xe being most undersaturated, through Kr, Ar, and N_2, to finally Ne being most supersaturated. We have not considered the effects of ocean-ice interactions in this model. The melting of ice shelves, such as in the southern Weddell Sea, is expected to impart a signature identical to complete bubble dissolution caused by breaking waves (Schlosser et al., 1990; Rodehacke et al., 2006; Severinghaus and Battle, 2006). We cannot distinguish between ice shelf melting and bubble-mediated air-sea gas exchange by gas observations alone. Freezing and melting of sea-ice may also have an impact on gas supersaturations (Hood, 1998; Hamme and Emerson, 2002). We argue that sea-ice meltwater would largely

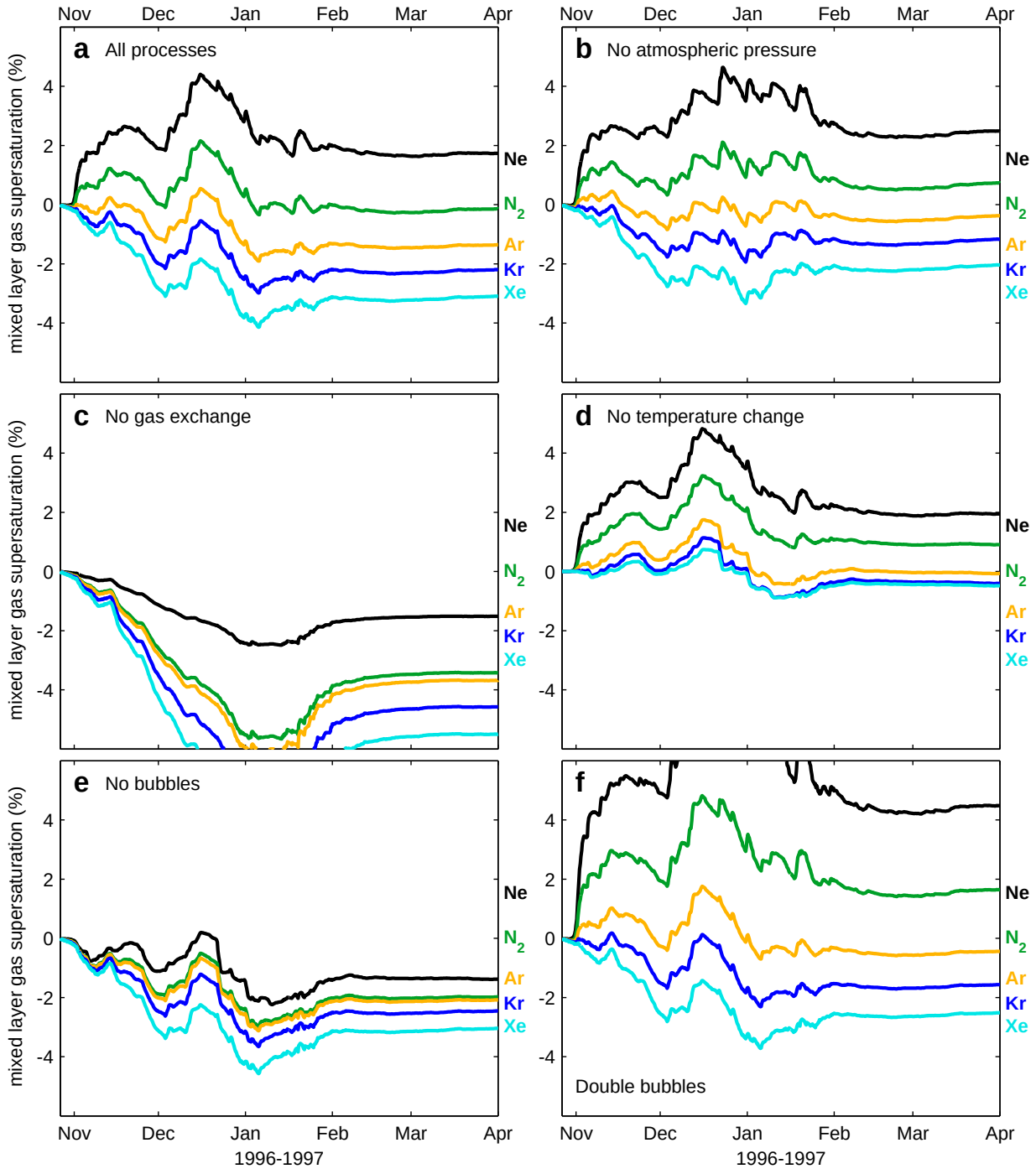

Figure 4: Evolution of gas supersaturations (in %) in the mixed layer for different model runs. The position of the gas labels near the right side of each graph indicates the mean gas supersaturations observed deeper than 2500m in the Pacific near Hawaii, including the 2% solubility offset for Xe. (a) All processes included in model run. (b) Model run with atmospheric pressure set to 1 atm. (c) Model run with neither diffusive nor bubble-mediated gas exchange. (d) Model run in which gas saturations did not respond to temperature changes. (e) Model run with no bubble-mediated gas exchange. (f) Model run with twice the normal rate of bubble-mediated gas exchange.

remain in a near surface layer that would have reequilibrated with the atmosphere by the end of summer. Ice formation in perennial ice-covered lakes has been shown to create intriguingly large deviations from equilibrium in dissolved gases (Hood et al., 1998). The magnitude of the effect on the open ocean is still uncertain (Postlethwaite et al., 2005; Well and Roether, 2003), but may be important where brine rejected from sea-ice freezing contributes to deep-water formation.

5 Conclusions

Our observations and model demonstrate that dissolved inert gases have the potential to be effective tracers of rapid cooling and air-sea gas exchange processes and may therefore have high utility for understanding gas dynamics during water mass formation. The model strongly suggests that the differences between the gases, rather than saturations of individual gases, will be most useful to constraining processes, because the differences are little affected by variable atmospheric pressure. We have shown that highly precise measurements of these gases can now be made at the 0.1–0.2% level. At present, high quality measurements of these gases have been made in very few locations around the world.

One of the benefits we see in making further measurements of these gases is in creating a dataset that can be used to constrain the efficiency of the solubility pump in ocean models. Krypton and Xe respond strongly to cooling and very little to bubbles, and so, despite solubility differences, these gases may be the best analogues for carbon dioxide, which is also temperature but not bubble sensitive. In this paper, the observed patterns of inert gases in the deep ocean have been explained using a purely seasonal model of wintertime convection in the Labrador Sea. The air-sea equilibration timescale of these inert gases is slow enough that the seasonal cycle can create several percent departures from equilibrium, but their equilibration timescale is still an order of magnitude faster than that of carbon dioxide. The degree to which inert gases can capture the dynamics of the carbon solubility pump will be controlled both by the importance to carbon dioxide of the seasonally-driven cooling during the winter just prior to subduction and by the extent to which inert gases are affected by cooling during sequential winters as water is transported to deep-water formation sites.

A Model Description

The model began with a temperature/salinity profile measured on October 26, 1996 at 56.76^{o}N 52.35^{o}W near the Bravo mooring. At this point, the mixed layer was warm (5.2 ^{o}C) and fresh (34.56 PSS), overlying remnant Labrador Sea Water (LSW) that was colder (2.7–3.1 ^{o}C) and saltier (34.84 PSS). At each 6-hour time step, the heat content of the slab mixed layer was adjusted based on the sum of short-wave, long-wave, sensible, and latent modified-NCEP heat fluxes (Figure 5a), obtained for this time period from G.W.K. Moore (Renfrew et al., 2002; Moore and Renfrew, 2002). Entrainment was forced when the density at the base of the mixed layer exceeded that of the layer directly below (1-m vertical resolution). For simplicity, shear-induced mixing and eddy diffusivity were not included in the model, though runs using the Price-Weller-Pinkel model (Price et al., 1986) suggested that including this process would not have changed our results significantly. We increased the total heat flux by 30% in order to match observed convection depths at the Bravo mooring (Lab Sea Group, 1998). Heat budgets from profiling floats also suggested that surface heat losses were greater than the modified-NCEP fluxes (Lavender et al., 2002; Steffen and D'Asaro, 2002). Reducing heat losses in the model to the Moore modified-NCEP levels resulted in shallower mixed layers and about half a percent higher final gas saturations but no change in the observed pattern of gas saturations. The simplifying assumption that the solar flux is confined to the mixed layer is justified by mixed layer depths greater than 85m throughout the model run and by low light levels. As the buoyancy effects of precipitation and evaporation seem to approximately balance in this region (Lab Sea Group, 1998), we made no surface flux adjustments to the salinity.

Diffusive gas exchange was calculated from the Moore dataset wind speed (Figure 5b) using the Nightingale et al. (2000) parameterization. We included sea level pressure (Figure 5c) in calculating the expected equilibrium gas concentrations, but not the effect of a cool skin (Robertson and Watson, 1992). Bubble-mediated gas exchange was treated as a separate process whose rate was proportional

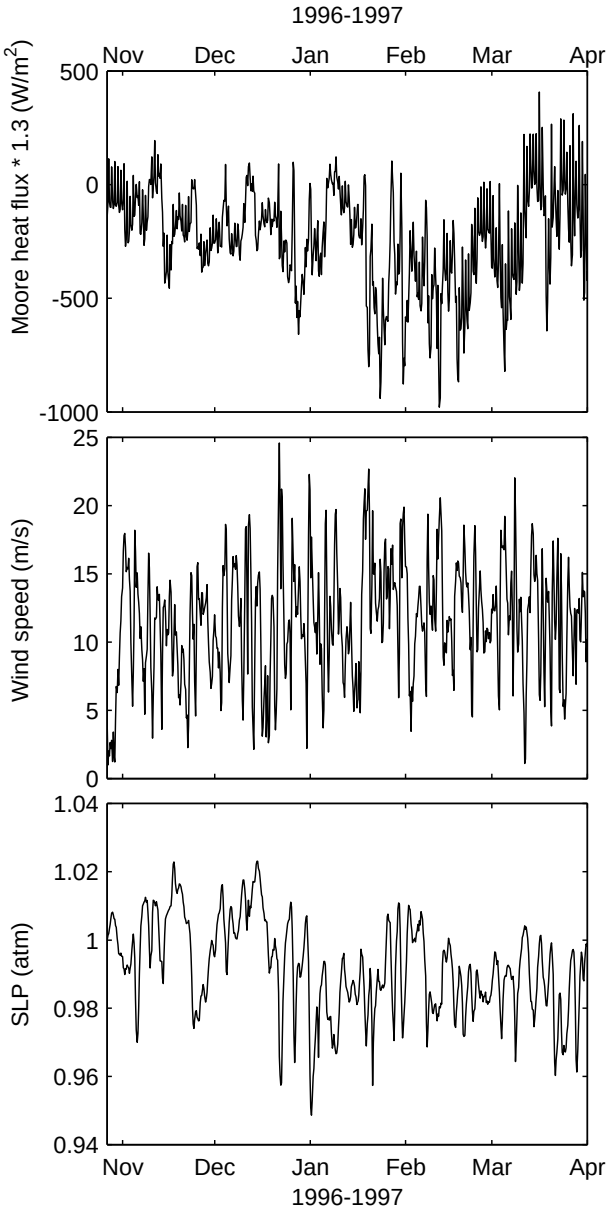

Figure 5: (a) Heat fluxes used to drive the model from the Renfrew et al. (2002) modified-NCEP fluxes, multiplied by 1.3. (b) Wind speeds (in m/s) and (c) sea level pressure (in atm) from the same dataset, used to determine diffusive gas exchange rates.

to the cube of the wind speed (Asher and Wanninkhof, 1998).

$$Bubble\,flux = V_{inj} * \chi_C * (u - 2.27)^3 \qquad (1)$$

where V_{inj} is a tunable parameter controlling the overall bubble flux rate, χ_C is the atmospheric mole fraction of some gas C, and u is the wind speed in m/s. Bubble fluxes were assumed to be zero at wind speeds less than 2.27 m/s, though these times were rare. Because the lack of observational gas data from this region does not justify a more complex bubble model for this simple thought experiment, we have assumed that the bubbles completely collapsed, injecting all of their contents into the water. Mass balance studies have shown that at least half of the bubble-mediated exchange of Ar in subtropical gyres occurs though completely collapsing bubbles (Hamme and Emerson, 2006; Stanley et al., 2006). High downward velocities observed by lagrangian floats in the Labrador Sea may force even more bubbles to depths at which they completely dissolve (Steffen and D'Asaro, 2002). The V_{inj} parameter was tuned to best reproduce the Ne supersaturation that we observed in the 3000-4600m range near Hawaii. Allowing half of the bubble-mediated gas exchange to occur through a large-bubble-dominated exchange mechanism (Hamme and Emerson, 2002), did not affect the pattern of gas saturations produced by the model and only raised the final saturation of the least bubble sensitive gases by about half a percent. The mean rate of bubble injection over the winter was 1.7 L air/m^2/d (median 1.3 with storm episodes up to 12 L air/m^2/d). For comparison, this rate was within a factor of two of the bubble fluxes derived by Hamme and Emerson (2006) and Emerson et al. (1995) for the subtropical North Pacific and by Stanley et al. (2006) and Spitzer and Jenkins (1989) for the subtropical North Atlantic.

The model run started in late October with gases at equilibrium with 1 atm pressure. In the mixed layer, the influence of this initial condition was erased within a few weeks. However, the initial gas saturations of the deeper waters, which were entrained as the water column convects in late winter, had an important effect on the final gas saturations of the water column. To reduce the importance of the gases' initial condition, we ran the model iteratively over eleven winters to reach a steady condition.

There is an additional complication, because the deeper water in the Labrador Sea at the beginning of the win-

ter is not only a product of the previous winter's convection. During the summer, warmer and saltier Irminger Sea Water (ISW) is mixed into the interior of the Labrador Sea from boundary currents (Cuny et al., 2002), altering the deep and uniform layer produced during the previous winter. To estimate the extent of this intrusion, we compared the initial temperature profile at the beginning of the winter with the final profile at the end of the winter, and calculated at each depth the mixing ratio of new ISW (4.5^oC) and water from the end of the previous winter's convection. Given these mixing ratios, we then calculated new initial conditions for the gases by assuming that new ISW had gas concentrations in equilibrium with the atmosphere, while the water from the previous winter's convection had gas saturations calculated by the previous year's model run. Wintertime cooling of water moving northward in the North Atlantic (McCartney and Talley, 1982) may cause this intruding ISW to be undersaturated with respect to the more temperature-sensitive dissolved gases, but we make here the simplest assumption possible that the gases are in equilibrium.

The temperature-based calculation of mixing ratios and the assumption of gas equilibrium in the ISW are weak points in the model. However, neither issue had an effect on the patterns of the gas saturations, our main focus in this paper. Both points are important to the amount that gas saturations rebound towards equilibrium in the latter half of the winter and are therefore important to the final saturations of individual gases predicted by the model. No addition of ISW resulted in final gas saturations that stayed near their early January levels, while resetting the entire water column to equilibrium with the atmosphere resulted in final saturations that were about half of our control run.

Acknowledgements

We wish to thank Steven Emerson, Charles Stump, and David Nicholson for collecting samples, sharing data with us, and loaning the sample bottles. Discussions with Ralph Keeling, Galen McKinley, Steven Emerson, and David Archer helped us to develop these ideas. We thank Melissa Headly and Ross Beaudette for analytical help in the lab. G.W.K. Moore provided meteorological data for the region. Jonathan Lilly provided CTD profile data, while Bravo mooring data from Peter Rhines and Jonathan Lilly was obtained at http://www.ldeo.columbia.edu/res/pi/labseacd/. Eric D'Asaro, Jonathan Lilly, Elizabeth Steffen, and Eleanor Williams advised us on convection in the Labrador Sea. Roberta was supported by the Gary Comer Abrupt Climate Change Fellowship and by NASA (ESS/99-0000-0022). NSF Office of Polar Programs (OPP 97-25305) and SIO Director's Office provided the Severinghaus lab mass spectrometer.

References

Archer, D. E., 2003. Argon concentration in the deep sea as an indicator of atmosphere/ocean CO_2 coupling and thermocline mixing. EOS Trans. AGU 84 (46), fall Meet. Suppl., Abstract OS22D-02.

Archer, D. E., Eshel, G., Winguth, A., Broecker, W., Pierrehumbert, R., Tobis, M., Jacob, R., 2000. Atmospheric pCO_2 sensitivity to the biological pump in the ocean. Global Biogeochemical Cycles 14 (4), 1219–1230.

Asher, W. E., Wanninkhof, R., 1998. The effect of bubble-mediated gas transfer on purposeful dual-gaseous tracer experiments. Journal of Geophysical Research 103 (C5), 10555–10560.

Benson, B. B., Krause, Jr., D., 1976. Empirical laws for dilute aqueous solution of nonpolar gases. Journal of Chemical Physics 64 (2), 689–709.

Benson, B. B., Parker, P. D. M., 1961. Nitrogen/argon and nitrogen isotope ratios in aerobic sea water. Deep-Sea Research 7 (4), 237–253.

Bieri, R. H., 1971. Dissolved noble gases in marine waters. Earth and Planetary Science Letters 10 (3), 329–333.

Bingham, F. M., Lukas, R., 1996. Seasonal cycles of temperature, salinity and dissolved oxygen observed in the Hawaii Ocean Time-series. Deep-Sea Research II 43 (2–3), 199–213.

Codispoti, L. A., Brandes, J. A., Christensen, J. P., Devol, A. H., Naqvi, S. W. A., Paerl, H. W., Yoshinari,

T., 2001. The oceanic fixed nitrogen and nitrous oxide budgets: Moving targets as we enter the anthropocene? Scientia Marina 65 (Suppl. 2), 85–105.

Craig, H., Weiss, R. F., 1971. Dissolved gas saturation anomalies and excess helium in the ocean. Earth and Planetary Science Letters 10 (3), 289–296.

Cuny, J., Rhines, P. B., Niiler, P. P., Bacon, S., 2002. Labrador Sea boundary currents and the fate of the Irminger Sea Water. Journal of Physical Oceanography 32 (2), 627–647.

Emerson, S., Quay, P., Karl, D., Winn, C., Tupas, L., Landry, M., 1997. Experimental determination of the organic carbon flux from open-ocean surface waters. Nature 389 (6654), 951–954.

Emerson, S., Quay, P. D., Stump, C., Wilbur, D., Schudlich, R., 1995. Chemical tracers of productivity and respiration in the subtropical Pacific Ocean. Journal of Geophysical Research 100 (C8), 15873–15887.

Emerson, S., Stump, C., Wilbur, D., Quay, P., 1999. Accurate measurement of O_2, N_2, and Ar gases in water and the solubility of N_2. Marine Chemistry 64 (4), 337–347.

Fuchs, G., Roether, W., Schlosser, P., 1987. Excess ^{3}He in the ocean surface layer. Journal of Geophysical Research 92 (C6), 6559–6568.

Fujieki, L. A., Santiago-Mandujano, F., Hannides, C., Lukas, R., Karl, D., 2006. Hawaii ocean time-series data report 15: 2003. Tech. rep., University of Hawaii, Honolulu, HI.

Fujieki, L. A., Santiago-Mandujano, F., Sheridan, C., Lukas, R., Karl, D., 2004. Hawaii ocean time-series data report 13: 2001. Tech. rep., University of Hawaii, Honolulu, HI.

Hamme, R. C., 2003. Applications of neon, nitrogen, argon and oxygen to physical, chemical and biological cycles in the ocean. Ph.D. thesis, University of Washington, USA.

Hamme, R. C., Emerson, S. R., 2002. Mechanisms controlling the global oceanic distribution of the inert gases argon, nitrogen and neon. Geophysical Research Letters 29 (23), 2120, doi:10.1029/2002GL015273.

Hamme, R. C., Emerson, S. R., 2004a. Measurement of dissolved neon by isotope dilution using a quadrupole mass spectrometer. Marine Chemistry 91 (1-4), 53–64.

Hamme, R. C., Emerson, S. R., 2004b. The solubility of neon, nitrogen and argon in distilled water and seawater. Deep-Sea Research I 51 (11), 1517–1528.

Hamme, R. C., Emerson, S. R., 2006. Constraining bubble dynamics and mixing with dissolved gases: Implications for productivity measurements by oxygen mass balance. Journal of Marine Research 64 (1), 73–95.

Hood, E. M., 1998. Characterization of air-sea gas exchange processes and dissolved gas/ice interactions using noble gases. Ph.D. thesis, MIT/WHOI.

Hood, E. M., Howes, B. L., Jenkins, W. J., 1998. Dissolved gas dynamics in perennially ice-covered Lake Fryxell, Antarctica. Limnology and Oceanography 43 (2), 265–272.

Ito, T., Deutsch, C., 2006. Understanding the saturation state of argon in the thermocline: the role of air-sea gas exchange and diapycnal mixing. Global Biogeochemical Cycles 20 (3), GB3019, doi: 10.1029/2005GB002655.

Jenkins, W. J., 1988. The use of anthropogenic tritium and helium-3 to study subtropical gyre ventilation and circulation. Philosophical Transactions of the Royal Society of London A 325 (1583), 43–61.

Karl, D. M., Lukas, R., 1996. The Hawaii Ocean Time-series (HOT) program: Background rationale and field implementation. Deep-Sea Research II 43 (2–3), 129–156.

Lab Sea Group, 1998. The Labrador Sea deep convection experiment. Bulletin of the American Meteorological Society 79 (10), 2033–2058.

Lavender, K. L., Davis, R. E., Owens, W. B., 2002. Observations of open-ocean deep convection in the Labrador Sea from subsurface ¤oats. Journal of Physical Oceanography 32 (2), 511–526.

Lide, D. R. (Ed.), 2002. CRC Handbook of Chemistry and Physics, 83rd Edition. CRC Press, Cleveland.

McCartney, M. S., Talley, L. D., 1982. The subpolar mode water of the North Atlantic Ocean. Journal of Physical Oceanography 12 (11), 1169–1188.

Moore, G. W. K., Renfrew, I. A., 2002. An assessment of the surface turbulent heat ¤uxes from the NCEP-NCAR reanalysis over the western boundary currents. Journal of Climate 15, 2020–2037.

Nightingale, P. D., Malin, G., Law, C. S., Watson, A. J., Liss, P. S., Liddicoat, M. I., Boutin, J., Upstill-Goddard, R. C., 2000. In situ evaluation of air-sea gas exchange parameterizations using novel conservative and volatile tracers. Global Biogeochemical Cycles 14 (1), 373–387.

Postlethwaite, C., Rohling, E., Jenkins, W., Walker, C., 2005. A tracer study of ventilation in the Japan/East Sea. Deep-Sea Research II 52 (11-13), 1684–1704.

Price, J. F., Weller, R. A., Pinkel, R., 1986. Diurnal cycling: Observations and models of the upper ocean response to diurnal heating, cooling, and wind mixing. Journal of Geophysical Research 91 (C7), 8411–8427.

Renfrew, I. A., Moore, G. W. K., Guest, P. S., Bumke, K., 2002. A comparison of surface layer and surface turbulent ¤ux observations over the Labrador Sea with ECMWF analyses and NCEP reanalyses. Journal of Physical Oceanography 32 (2), 383–400.

Robertson, J. E., Watson, A. J., 1992. Thermal skin effect of the surface ocean and its implication for CO_2 uptake. Nature 358 (6389), 738–740.

Rodehacke, C. B., Hellmer, H. H., Huhn, O., Beckmann, A., 2006. Ocean/ice shelf interaction in the southern Weddell Sea: Results of a regional numerical helium/neon simulation. Ocean Dynamics 57 (1), 1–11.

Sarmiento, J., Murnane, R., LeQuéré, C., 1995. Air-sea CO_2 transfer and the carbon budget of the North Atlantic. Philosophical Transactions of the Royal Society of London B 348 (1324), 211–219.

Schlosser, P., Bayer, R., Foldvik, A., Gammelsrød, T., Rohardt, G., Münnich, K., 1990. Oxygen 18 and Helium as tracers of ice shelf water and water/ice interaction in the Weddell Sea. Journal of Geophysical Research 95, 3253–3263.

Severinghaus, J. P., Battle, M. O., 2006. Fractionation of gases in polar ice during bubble close-off: New constraints from £rn air Ne, Kr and Xe observations. Earth and Planetary Science Letters 244 (1-2), 474–500.

Severinghaus, J. P., Grachev, A. M., Luz, B., Caillon, N., 2003. A method for precise measurement of argon 40/36 and krypton/argon ratios in trapped air in polar ice with applications to past £rn thickness and abrupt climate change in Greenland and at Siple Dome, Antarctica. Geochimica et Cosmochimica Acta 67 (3), 325–343.

Spitzer, W. S., Jenkins, W. J., 1989. Rates of vertical mixing, gas exchange and new production: Estimates from seasonal gas cycles in the upper ocean near Bermuda. Journal of Marine Research 47 (1), 169–196.

Stanley, R. H. R., Jenkins, W. J., Doney, S. C., 2006. Quantifying seasonal air-sea gas exchange processes using noble gas time-series: A design experiment. Journal of Marine Research 64, 267–295.

Steffen, E. L., D'Asaro, E. A., 2002. Deep convection in the Labrador Sea as observed by lagrangian ¤oats. Journal of Physical Oceanography 32 (2), 475–492.

Takahashi, T., Takahashi, T. T., Sutherland, S. C., 1995. An assessment of the role of the North Atlantic as a CO_2 sink. Philosophical Transactions of the Royal Society of London B 348 (1324), 143–152.

Talley, L. D., 1997. North Pacific Intermediate Water transports in the mixed water region. Journal of Physical Oceanography 27, 1795–1803.

Toggweiler, J. R., Gnanadesikan, A., Carson, S., 2003. Representation of the carbon cycle in box models and GCMs: 1. Solubility pump. Global Biogeochemical Cycles 17 (1), 1026, doi:10.1029/2001GB001401.

Weiss, R. F., Kyser, T. K., 1978. Solubility of krypton in water and seawater. Journal of Chemical and Engineering Data 23 (1), 69–72.

Well, R., Roether, W., 2003. Neon distribution in South Atlantic and South Pacific waters. Deep-Sea Research I 50 (6), 721–735.

Wood, D., Caputi, R., 1966. Solubilities of Kr and Xe in fresh and sea water. Tech. rep., U.S. Naval Radiological Defense Laboratory, San Francisco, CA.

Woolf, D. K., Thorpe, S. A., 1991. Bubbles and the air-sea exchange of gases in near-saturation conditions. Journal of Marine Research 49 (3), 435–466.